J. Wind Eng. Ind. Aerodyn. 134 (2014) 109–121

Contents lists available at ScienceDirect

Journal of Wind Engineering and Industrial Aerodynamics

journal homepage: www.elsevier.com/locate/jweia

Direct-forcing immersed boundary modeling of vortex-induced vibration of a circular cylinder

Ming-Jyh Chern [a,b,*], Yu-Hao Kuan [a], Giri Nugroho [c], Guan-Ting Lu [a], Tzyy-Leng Horng [d]

[a] Department of Mechanical Engineering, National Taiwan University of Science and Technology, 43 Sec. 4 Keelung Road, Taipei 10607, Taiwan
[b] Ocean Technology Research Center, National Taiwan University, Taipei 10617, Taiwan
[c] Department of Mechanical Engineering, Institute Teknologi Sepuluh Nopember, Sukolilo, Surabaya 60111, Indonesia
[d] Department of Applied Mathematics, Feng Chia University, Taichung 40724, Taiwan

ARTICLE INFO

Article history:
Received 30 March 2014
Received in revised form
27 August 2014
Accepted 27 August 2014

Keywords:
Direct-forcing immersed boundary method
Vortex shedding
Vortex-induced vibration
Lock-in
Synchronization

ABSTRACT

A numerical study of the vortex-induced vibration (VIV) of a flexible supported circular cylinder using the direct-forcing immersed boundary (DFIB) method incorporating the virtual force term is investigated. The use of DFIB method eliminates the requirement of mesh regeneration at each time step, owing to the movement of the cylinder, a practice which is common with body-fitted grid setups. The fluctuating hydrodynamic forces may cause the vibration of the structure due to vortex shedding behind it. In reality, this vibration phenomenon may result in the failure of the structure especially for the so-called lock-in/synchronization phenomenon. The present study shows that a dynamically mounted circular cylinder is allowed to vibrate transversely only or both in the in-line and the transverse directions in a uniform flow at a moderate Reynolds number. The effects of reduced velocity and gap ratio on VIV are discussed. Hydrodynamic coefficients of a freely vibrating cylinder are analyzed in time and spectral domains. The cylinder orbits the slightly oval-shaped and eight-shaped motions in the lock-in regime. Moreover, the 2S and the C(2S) vortex shedding modes can be found at the low amplitude vibration and the large amplitude vibration, respectively. The comparisons against the published data prove the capability of the present DFIB model. This proposed model can be useful for the investigation of VIV of the structures.

1. Introduction

Vortex-induced vibration (VIV) of a structure has become an important issue in many engineering areas, such as aerospace engineering, civil engineering, wind engineering, and ocean engineering. For aerospace engineering, an airfoil subject to the fluttering would be damaged due to the large amplitude vibrations. In the civil engineering and the wind engineering, it may cause galloping of bridges and chimneys due to the interaction with current and wind, respectively. For an offshore application, such as submerged pipelines on a seabed may vibrate acutely due to ocean currents. It results in the damage of flexible risers in petroleum production.

VIV has been regarded as one of the dominating causes for the fatigue failure to the structures. However, this phenomenon could be very useful in renewable energy as well. The kinetic energy of the vibrating structure, which comes from the flow, can be converted to usable electric energy given that a proper power take-off (PTO) mechanism is designed to link the structure and the power generator. Recently, Bernitsas et al. (2008) developed a VIVACE (Vortex-induced vibrations for aquatic clean energy) machine that can harvest energy from most of the water currents around a vibrating structure. Actually, VIV problems are always complicated and exit in situations such as inclined and free shear flows, the effects of turbulence and rigid plane boundary, regular or irregular wave, and so on. To further realize VIV phenomena, the prediction of the amplitude and frequency responses of a vibrating circular cylinder is necessary.

It is well known that VIV exists under the action of unsteady hydrodynamic forces arising from alternative vortex shedding behind a solid body immersed in fluid flow. As vortices shed, the periodic forces exert on the solid body in a flow field. Considering an elastically mounted circular cylinder, the periodic forces lead to the movement of the cylinder. Under certain conditions, the vortex-shedding frequency is close to its natural frequency and then self-excited vibrations would be induced. This phenomenon is referred as lock-in/synchronization which may cause the failure of the structure, especially for the resonance case. The practical significance of VIV has led to a large number of fundamental studies.

* Corresponding author at: Department of Mechanical Engineering, National Taiwan University of Science and Technology, 43 Sec. 4 Keelung Road, Taipei 10607, Taiwan. Tel.: +886 2 27376496; fax: +886 2 27376460.
E-mail address: mjchern@mail.ntust.edu.tw (M.-J. Chern).

http://dx.doi.org/10.1016/j.jweia.2014.08.015
0167-6105/

Nomenclature

English Symbols

A	dimensionless amplitude
c	structural damping, N s m^{-1}
d_x, d_y	displacements in the in-line and the transverse directions, m
D	diameter of cylinder, m
$\mathbf{f}^*$	dimensionless virtual force per unit mass
f_n	natural frequency of structure, s^{-1}
f_v	frequency of vortex shedding, s^{-1}
f_n^*	dimensionless natural frequency of structure
f_v^*	dimensionless frequency of vortex shedding
$\mathbf{F}$	total dimensionless virtual force
I, J	numbers of grid points in the x- and y-directions
k	structural stiffness, N m^{-1}
L	axial length of structure, m
m^*	dimensionless mass ratio
m_s	structural mass of solid, kg
p	dimensionless pressure
Re	Reynolds number, $u_\infty D/\nu$
St	Strouhal number, $f_v D/u_\infty$
t	time, s
t^*	dimensionless time
$\mathbf{u}$	dimensionless velocity of fluid
$\mathbf{u}'$	dimensionless first intermediate velocity
$\mathbf{u}''$	dimensionless second intermediate velocity
$\mathbf{u}_s$	dimensionless velocity of solid
u_∞	free stream velocity, m s^{-1}
U_R^*	dimensionless reduced velocity
x, y	horizontal and vertical cartesian coordinates
X, Y	dimensionless displacements in the in-line and the transverse directions

Greek Symbols

η	dimensionless fraction of volume cells
ν	kinematic viscosity of fluid, m^2 s^{-1}
ρ	density, kg m^{-3}
ζ	dimensionless damping ratio of structure
$\mathcal{D}$	convergence criterion

Subscripts

f	fluid
s	solid

Superscripts

n	time step level
$*$	dimensionless parameter
$'$	first intermediate time step level
$''$	second intermediate time step level

Many of them are discussed in comprehensive reviews of the investigations on various aspects of VIV such as Sarpkaya (1979), Bearman (1984), Parkinson (1989) and Williamson and Govardhan (2004). Some literatures claim that a combined mass-damping parameter ($m^*\zeta$) controls the cylinder responses of the VIV system. Herein, m^* is the ratio of the structure mass to fluid mass and ζ is the structural damping. Feng (1968) conducted a well-known experiment on cross-flow vibration of a flexibly mounted circular cylinder in air flow with high $m^*\zeta$. In his study, it demonstrates a typical lock-in phenomenon and the occurrence of resonance of the cylinder over a range of reduced velocity U_R^*. Two amplitude response branches such as the initial and the lower branches exist given that $m^*\zeta$ is high as explained by Khalak and Williamson (1996) and Govardhan and Williamson (2000). Brika and Laneville (1993) studied cases of aeroelastics for a slender cylinder with low $m^*\zeta$ in a wind tunnel. In terms of their flow visualization results, it turns out that the initial branch of the hysteresis loop is associated with the 2S (two single vortices released per cycle) mode and the lower branch with the 2P (two vortex pairs shed per cycle) mode. The experimental studies involving the transverse vibration of an elastically mounted circular cylinder with extraordinarily low $m^*\zeta$ in a water channel was undertaken by Khalak and Williamson (1996, 1997a,b, 1999).For low $m^*\zeta$, three response modes, initial, upper, and lower modes, were reported. They indicated that the transition between the initial and upper response branches involves a hysteresis. This contrasts with the intermittent switching of modes for the transition between the upper and lower branches. In the upper branch, it is also found that the 2P mode exists but the resonant amplitude is distinctly higher than other two branches. Guilmineau and Queutey (2004) reported numerical simulations for the transverse vibration of a flexibly mounted circular cylinder with low $m^*\zeta$ in turbulent flow. In their study, three initial conditions were considered: rest, increasing velocity, and decreasing velocity. It is showed that the simulations predict only the lower branch under rest and decreasing velocity. On the other hand, with the increasing velocity condition, the upper branch is predicted. Blevins and Coughran (2009) conducted experimental investigations in one and two dimensional VIV of an aeroelastic circular cylinder with various m^* and ζ in turbulent water flow.They pointed out that the in-line frequency is approximately twice the transverse frequency and the two-degree-of-freedom cylinder orbits an eight-shaped motion.

The advantages for predicting physical phenomena in advance and reducing the cost have been generally accepted in computational fluid dynamics (CFD). The immersed boundary (IB) method is a novel numerical methodology for the simulation of fluid–structure interaction problems due to its capability to handle simulations for a moving boundary with less computational cost and memory requirements than the conventional body-fitted method since it was introduced by Peskin (1972). The IB method includes a virtual force in the Navier–Stokes equations to express the effect of fluid–structure interaction. An alternative IB method named the direct-forcing method was introduced by Mohd. Yusof (1996). Instead of using a velocity interpolation to distribute the force from a Lagrangian grid to an Eulerian grid, Noor et al. (2009) used the so-called volume of solid function to link the force in the fluid–structure interaction. It does not require re-meshing for moving body problems at each time step since it uses the Cartesian grids. The idea of the direct-forcing immersed boundary (DFIB) method has been adopted and obtained successful applications. Wang et al. (2008) conducted a multi-DFIB method for the modeling of the hitting and rebounding process of the single particle sedimentation and the sedimentation of multi-particles. Their quantitative comparisons against other studies of the flows laden with moving particles validated their model. Luo et al. (2012) developed a hybrid formulation using an IB method which represents for the association between the solid body surface and the local flow reconstruction to the validations including two- and three-dimensional, stationary, and moving boundaries. This approach can suppress the force oscillations and computational cost for the numerical

oscillation occurring in the moving boundary problems. Lee and You (2013) studied an IB method based on a ghost-cell method coupled with a mass source/sink algorithm for reducing spurious force oscillations in moving body problems. They found that the magnitude of spurious force oscillations is proportional to the grid spacing and is inversely proportional to the time increment. Sotiropoulos and Yang (2014) reviewed a variety of immersed boundary methods and reported recent results from the application of immersed boundary methods. Various fluid–structure interaction problems such as vortex induced vibrations, aquatic swimming, and so on, which were solved by immersed boundary methods were shown and explained in their review article.

The present numerical method involving a combined DFIB method with a volume of solid function is established. It is used to predict the flow characteristics of the dynamic responses of VIV for an elastically mounted circular cylinder in a uniform flow. The flow characteristics are analyzed using the variation of the maximum displacement of cylinder center and the fluctuating hydrodynamic coefficients. Also, the vortex shedding modes, frequency responses and the trajectory diagrams are predicted. Simulations of a freely vibrating circular cylinder in the in-line and the transverse directions under a uniform flow at moderate *Re* are carried out.

2. Mathematical formulae and numerical methods

In this study, the direct-forcing immersed boundary (DFIB) and the finite volume method are utilized to establish the proposed numerical model. The DFIB method adds a virtual force in the incompressible Navier–Stokes equations to simulate the fluid–structure interaction. The DFIB method has been applied to various problems of fluid–structure interaction successfully (see Noor et al., 2009; Chern et al., 2012, 2013). More details about the DFIB method are described in the following.

2.1. Governing equations and direct-forcing immersed boundary method

Flow past an elastically mounted circular cylinder is illustrated in Fig. 1. The circular cylinder vibrates in two-degree-of-freedom due to vortex shedding behind it. The free stream in the present study is parallel to the plane boundary. The distance between the inlet and the cylinder in the present model is enough to transform the free stream into a fully developed flow. The non-dimensional continuity and momentum equations governing incompressible fluid flow are expressed as

$$\nabla \cdot \mathbf{u} = 0 \tag{1}$$

and

$$\frac{\partial \mathbf{u}}{\partial t^*} + \nabla \cdot (\mathbf{uu}) = -\nabla p + \frac{1}{Re}\nabla^2 \mathbf{u} + \mathbf{f}^* \tag{2}$$

where $\mathbf{u}$ and p are non-dimensional velocity and pressure, respectively. $\mathbf{u}$ is nondimensionalized by u_∞ which is the inlet free stream velocity and used as the characteristic velocity. *Re* is the Reynolds number given by $u_\infty D/\nu$ where D is the cylinder diameter, ν is the kinematic viscosity of fluid, and $\mathbf{f}^*$ is the dimensionless virtual force term. In general, there are two different IB methods to handle complex geometries. One of the IB methods is to use a regular Eulerian computational grid for the fluid and a Lagrangian representation of the immersed boundary. This IB method was first proposed by Peskin (1972). The interaction between the fluid and the immersed elastic structure is expressed in terms of spreading and interpolation operations by use of smoothing Dirac delta functions. The alternative IB method

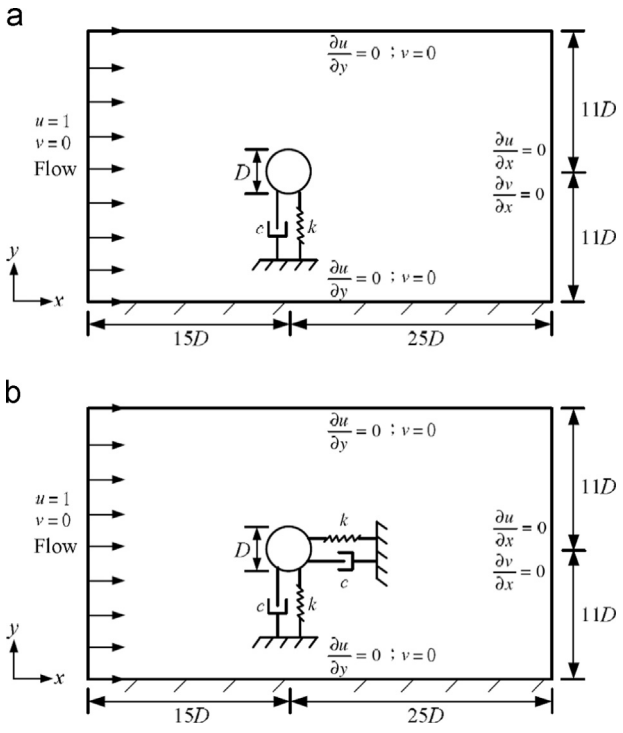

Fig. 1. Problem description and boundary conditions for VIV of an elastically mounted circular cylinder: (a) transverse vibration and (b) in-line and transverse vibrations.

is the direct-forcing method proposed by Mohd. Yusof (1996) and adopted in the present study. The forcing term $\mathbf{f}^*$ is determined by the difference between the interpolated velocity on the boundary point and the desired boundary velocity. It is determined by

$$\mathbf{f}^* = \eta \frac{\mathbf{u}_s - \mathbf{u}''}{\Delta t}. \tag{3}$$

Herein, $\mathbf{u}_s$ and $\mathbf{u}''$ are denoted as the solid velocity of cylinder center and the second intermediate velocity. The solid body is identified by a volume-of-solid function, η. It denotes a fraction of solids within a cell where η is equal to 1 and 0 for solid and fluid cells, respectively, and be fractional in boundary cells. Nevertheless, η is either 1 or 0 only and the fractional value is ignored in this study. For example, the circular cylinder is considered in the computational domain. The term η is 1 if the distance between the center of the cylinder and the center of a cell is less than the radius of the cylinder. Otherwise, η is 0 given that the distance is greater than the radius of the cylinder.

2.2. The equations of motion for a vibrating rigid body

For the VIV problems considered in this study, the moving structure is assumed to be rigid and mounted on elastic bases that allow displacements in the in-line and transverse directions. Such behavior of a vibrating structure can be described by the equation of a mass–damper–spring system forced by the hydrodynamic loading. The velocity and the position of the cylinder center have to be computed from the instantaneous hydrodynamic forces that exert on a solid body according to the Newton's second law of motion. The motion of the solid body in the two dimensional Cartesian coordinate system is governed by the following dimensionless equations:

$$\ddot{X} + \frac{4\pi\zeta}{U_R^*}\dot{X} + \left(\frac{2\pi}{U_R^*}\right)^2 X = \frac{2C_D(t^*)}{\pi m^*} \tag{4}$$

Table 1
Non-dimensional groups.

Time	t^*	$\frac{tu_\infty}{D}$
In-line displacement	X	$\frac{d_x}{D}$
Transverse displacement	Y	$\frac{d_y}{D}$
Mass ratio	m^*	$\frac{4m_s}{\pi\rho_f D^2 L}$
Reduced velocity	U_R^*	$\frac{u_\infty}{f_n D}$
Structural damping ratio	ζ	$\frac{c}{2\sqrt{m_s k}}$
Reduced natural frequency	f_n^*	$\frac{f_n D}{u_\infty}$

Herein, u_∞ is free stream velocity. The terms d_x and d_y are the displacements of cylinder center in the x- and y-directions. Relevant structural parameters are solid mass m_s, structural damping c and structural stiffness k. The term f_n is the natural frequency of the structure and L is the axial length of the structure.

and

$$\ddot{Y}+\frac{4\pi\zeta}{U_R^*}\dot{Y}+\left(\frac{2\pi}{U_R^*}\right)^2 Y=\frac{2C_L(t^*)}{\pi m^*} \tag{5}$$

where $\ddot{X}$, $\dot{X}$ and X are the normalized in-line acceleration, velocity and displacement of the center of a circular cylinder, respectively, while $\ddot{Y}$, $\dot{Y}$ and Y are the same quantities in the transverse direction. U_R^* is the reduced velocity of the system. The term ζ is the structural damping ratio. The term m^* is the mass ratio of solid to liquid mass while $C_D(t^*)$ and $C_L(t^*)$ are the instantaneous drag and lift coefficients, respectively. After instantaneous C_D and C_L are determined at each time step, the fourth-order Runge–Kutta algorithm is employed to solve Eqs. (4) and (5). The dimensionless group associated with Eqs. (4) and (5) can be found in Table 1. In the present work, the diameter of cylinder D is used as the characteristic length. In the study of two-degree-of-freedom vibrations, the structural stiffness and the structural damping are assumed to be isotropic.

2.3. Numerical methods for solving the Navier–Stokes equations

The DFIB method can handle complex geometry problem using a simple Cartesian grid. The finite volume method is applied to solving the Navier–Stokes equations in those grids. Therefore, the spatial and temporal discretizations using a number of numerical schemes are discussed in the following.

2.3.1. Spatial and temporal discretizations

In this paper, the diffusive and the convective terms of Eq. (2) are discretized using the second-order central difference scheme and the third-order quadratic upstream interpolation for convective kinetics (QUICK) scheme proposed by Leonard (1979), respectively. A staggered grid is used in the present work. For the temporal terms, the Adam–Bashforth scheme is applied. This scheme can ensure the third-order accuracy of time integral. The first intermediate velocity $\mathbf{u}'$ is calculated first by solving the advection–diffusion equations without the pressure gradient and virtual force term

$$\mathbf{u}'=\mathbf{u}^n+\frac{\Delta t^*}{12}[23S^n-16S^{n-1}+5S^{n-2}] \tag{6}$$

where S includes the diffusive and convective terms of Eq. (2) at each time step. The third-order Adam–Bashforth temporal scheme is implemented to predict the first intermediate velocity in Eq. (6).

2.3.2. Prediction–correction for pressure–velocity

In general, the first intermediate velocity in Eq. (6) does not satisfy the continuity equation. At the second step the first intermediate velocity is advanced by including the pressure term

$$\mathbf{u}''=\mathbf{u}'-\Delta t^*\nabla p^{n+1} \tag{7}$$

Taking the divergence for both sides of Eq. (7) gives

$$\nabla\cdot\mathbf{u}''=\nabla\cdot\mathbf{u}'-\Delta t^*\nabla^2 p^{n+1}. \tag{8}$$

Subsequently, the second intermediate velocity $\mathbf{u}''$ would satisfy the mass conservation

$$\nabla\cdot\mathbf{u}''=0. \tag{9}$$

Substitution of Eq. (9) into Eq. (8) gives the Poisson equation of pressure

$$\nabla^2 p^{n+1}=\frac{1}{\nabla t^*}\nabla\cdot\mathbf{u}'. \tag{10}$$

At the second step, the second intermediate velocity $\mathbf{u}''$ in Eq. (7) can be determined after solving the Poisson equation in Eq. (10) by the SOLA algorithm proposed by Hirt et al. (1975). This scheme uses an iterative method on the pressure field to conserve the continuity equation. At each time step, pressure at each cell is updated iteratively by adjusting the tentative velocities to satisfy a required tolerance.

Finally, the virtual force term representing the effect of a solid body on fluid should be included at the third step, so the final velocity $\mathbf{u}^{n+1}$ can be obtained by imposing the virtual force term as follows:

$$\mathbf{u}^{n+1}=\mathbf{u}''+\Delta t^*\mathbf{f}^{*n+1}. \tag{11}$$

The dimensionless virtual force $\mathbf{f}^{*n+1}$ reveals the existence of a force to hold or drive a solid body when it is stationary or moving. It can be defined from the rate of momentum changes of a solid body and proportional to the difference between the solid velocity at the $(n+1)$th time step and the local fluid velocity at the (n)th time step. To satisfy the no-slip boundary condition at the fluid–solid interface, it should be ensured that the fluid velocity $\mathbf{u}^{n+1}$ is equal to the solid velocity $\mathbf{u}_s^{n+1}$. The force exits on the solid body and zero elsewhere. Furthermore, it can be simply written as

$$\mathbf{f}^{*n+1}=\eta\frac{\mathbf{u}^{n+1}-\mathbf{u}''}{\Delta t^*}=\eta\frac{\mathbf{u}_s^{n+1}-\mathbf{u}''}{\Delta t^*}. \tag{12}$$

On account of the free oscillations of a circular cylinder, the solid velocity $\mathbf{u_s}$ can be obtained from Eqs. (4) and (5), respectively.

In this study, the integral of the virtual force is the dimensionless resultant force exerted on a circular cylinder by using the Simpson's 1/3 rule.

$$\mathbf{F}=\int\int\int_\Omega \mathbf{f}^*\,dV, \tag{13}$$

where $\mathbf{F}$ are the resultant of total dimensionless virtual forces. The dimensionless in-line and transverse force coefficients, C_D and C_L can be denoted as

$$C_D=-2F_x \tag{14}$$

and

$$C_L=-2F_y \tag{15}$$

respectively. The time average of in-line and root-mean-square value of transverse forces in dimensionless form are defined as

$$\overline{C}_D=\frac{1}{t}\int_0^t C_D\,dt \tag{16}$$

and

$$C_{L,rms} = \left(\frac{1}{t}\int_0^t C_L^2\, dt\right)^{1/2} \tag{17}$$

respectively.

2.4. Procedures for fluid–structure interaction

The complete numerical procedures for each time step of the proposed DFIB method are summarized in the following algorithm.

1. Identify the immersed boundary location and determine the volume-of-solid function η at each cell.
2. Compute the first intermediate velocity $\mathbf{u}'$ by Eq. (6) including the diffusive and convective terms.
3. Reconstruct the pressure gradient by solving the Poisson equation associated with Eq. (10), then advance the intermediate velocity $\mathbf{u}''$ by Eq. (7) to satisfy the mass conservation.
4. Solve the virtual force in the entire domain by means of Eq. (12). Thus, the total hydrodynamic force acting on the solid, the drag and lift coefficients can be obtained from Eqs. (13), (14) and (15), respectively.
5. Update flow field velocity $\mathbf{u}^{n+1}$ using the calculated virtual force by Eq. (11).
6. Calculate the solid motion described in Eqs. (4) and (5) to get the velocity and displacement of solid. If the solid is fixed, then $\mathbf{u_s}$ will be always zero.

2.5. Computational domain and computing time

The computational domain of $40D \times 22D$ for simulations of 1-DOF and 2-DOF VIV problems is discretized into $I \times J = 239 \times 169$ non-uniform grids while $60D \times 20D$ for modeling of a 2-DOF vibrating circular cylinder close to a rigid boundary problem is discretized into $I \times J = 445 \times 197$ non-uniform grids. The computational domain is considered as Cartesian grids. The grid spacing at the ith node is given by the expression proposed by Kuyper et al. (1993)

$$x_i = \frac{i}{i_{max}} - \frac{k}{\theta}\sin\left(\frac{i\theta}{i_{max}}\right) \tag{18}$$

Herein, $\theta = 2\pi$ stretches both ends of the domain whereas $\theta = \pi$ clusters more grid points near one end of the domain. The term k varies between 0 and 1. When it approaches 1 more points fall near the end. For the vicinity of the cylinder, the grid space is uniform. More details about the grid configuration and computational domain are presented in Fig. 2. In the beginning of simulations, the region of the cylinder oscillation is predicted in about 1.2D and 2D in the in-line and transverse directions, respectively.

The purpose using a non-uniform grid configuration is to increase the accuracy of the present method and to accurately capture the VIV phenomenon. When free oscillations are considered, since an explicit scheme is used to treat the unsteady problems, in order to avoid instability, the time increment is set as $\Delta t^* = 10^{-3}$ to satisfy the Courant–Friedrichs–Lewy (CFL) number. Herein, the CFL number is always less than 0.1 in the present study. Also, the mass convergence criterion at each time step is set as $\mathcal{D} = 10^{-4}$. The longest simulation takes at least 20 days to reach the dimensionless time $t^* = 1000$ which happens in the problem of a 2-DOF circular cylinder close to a rigid boundary at a PC cluster consisting of Intel Xeon E31220 processors 3.10 GHz.

2.6. Grid independence and validation of in-house numerical code

In the numerical study by Noor et al. (2009), a uniform flow past a stationary cylinder using the current DFIB method at $Re = 40$ and 100 was performed successfully. In their results, the time history of recirculation length at $Re = 40$, $\overline{C}_D$ and St of the cylinder at $Re = 100$ have good agreement with other literatures. The numerical prediction of cylinder array in oscillatory flow by Chern et al. (2012, 2013) has accomplished successfully using the same DFIB method. The oscillatory flow around a cylinder array in a square arrangement was simulated and validated by the in-line force coefficient C_f of the interaction of oscillatory flow with a single circular cylinder at moderate Keulegan–Carpenter numbers $KC = 2$ and 10. In terms of those studies, it turns out that the proposed DFIB method is capable of simulating fluid–solid interactions and of predicting hydrodynamic loadings on cylinders properly. In order to ensure that the numerical results are grid independent especially for free vibrations of a circular cylinder, several grid configurations are utilized to simulate the transverse oscillations of a circular cylinder. In this case, the flow and structural parameters are chosen according to Leontini et al. (2006) ($Re = 200$, $m^* = 10$, $\zeta = 0.01$ and $U_R^* = 3.5$). Since the proposed model is established for an unsteady flow, it is interesting to investigate the influence of the grid from the flow evolution. Four various corresponding smallest grid spacings of these meshes (0.1D, 0.05D, 0.025D and 0.020D) are allocated in the vicinity of the cylinder. The results for the grid independent study are shown in Fig. 3. As Fig. 3 presents, the time histories of the normalized

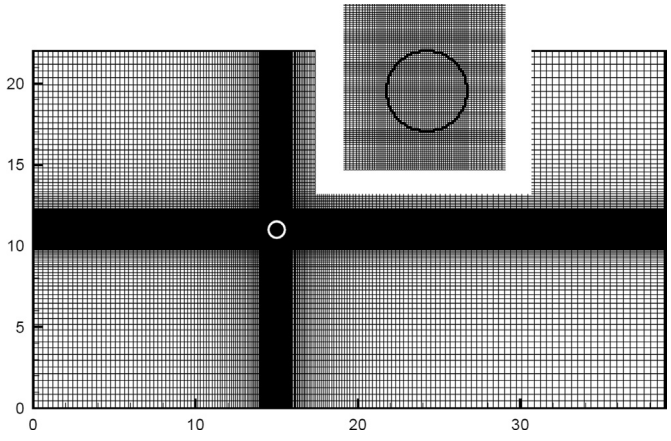

Fig. 2. The grid configurations for VIV of an elastically mounted circular cylinder.

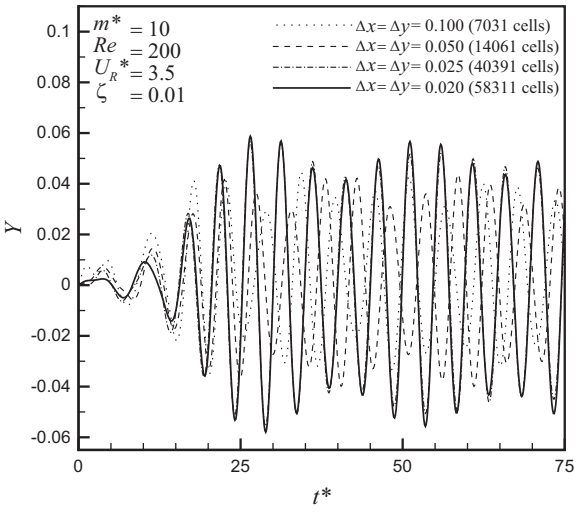

Fig. 3. The grid independent tests of time history of the normalized transverse displacement of the vibrating cylinder.

transverse displacement given by $\Delta x = \Delta y = 0.025$ and 0.02 are very similar and overlap with each other. Therefore, for advancing the accuracy of numerical results and saving the computational time, the grid spacing $\Delta x = \Delta y = 0.025$ in the vicinity of the vibrating cylinder is adopted in the present work. Herein, a total number of 1257 uniform grid cells are used to describe the vibrating cylinder.

3. Results and discussion

It is well known that vortex-induced-vibration (VIV) of an elastically mounted circular cylinder is affected by a group of parameters including mass ratio m^*, reduced velocity U_R^*, structural damping ratio ζ, Reynolds number Re, and so on. A parametric study is undertaken to investigate the influences of U_R^* on the amplitude and frequency responses of the cylinder. In order to investigate the capability of the present direct-forcing immersed boundary (DFIB) model and to predict basic response of a vibrating cylinder, two various cases are implemented. In the first case, the vibrating cylinder freely vibrates in the transverse direction as shown in Fig. 1(a). In the second case, the vibrating cylinder freely vibrates in both the transverse and in-line directions as shown in Fig. 1(b).

3.1. Transverse vibration

In this study, a uniform flow past an elastically mounted circular cylinder undergoing single-degree-of-freedom vibrations is first simulated and the numerical results are compared with the numerical data by Dettmer and Peric (2006). They used the Arbitrary Lagrangian Eulerian (ALE) method in this topic. The computational domain is $40D \times 22D$ and the illustration including boundary conditions is shown in Fig. 1(a). In this validation study, the $0.025D$ mesh size is utilized to simulate the single-degree-of-freedom problem. In order to facilitate the proposed model, the simulation parameters are set as same as in the numerical study of Dettmer and Peric (2006). The mass ratio $m^* = 149.1$, the damping ratio $\zeta = 0.0012$, and the natural frequency $f_n = 7.016$ are used in the study. The reduced velocity U_R^* varies in the interval between 5.0 and 7.2. The change of U_R^* is achieved by altering the flow velocity, so Re is also changed. Re/U_R^* is kept at a constant of 17.96. Simulations are carried out for Re ranging from 90 to 130 and a fast Fourier transform (FFT) technique of C_L is applied to determining the vortex shedding frequency in each case.

The time history of the normalized transverse displacement of the vibrating cylinder for various values of U_R^* is presented in Fig. 4. As a result, the waveform of beating grows in each cycle and the vibration amplitude increases gradually before it reaches a

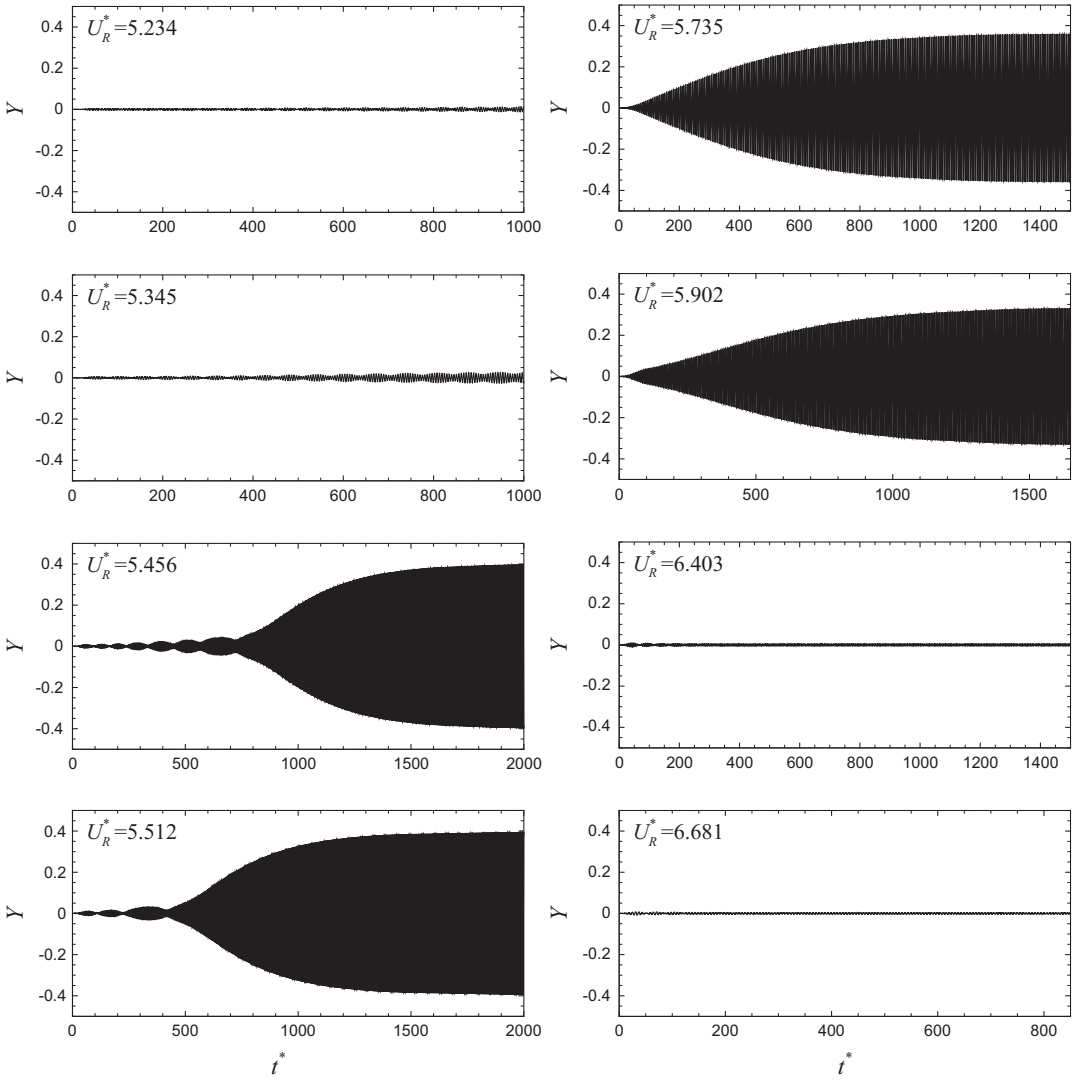

Fig. 4. Time history of the normalized transverse displacement of the vibrating cylinder for various values of reduced velocity.

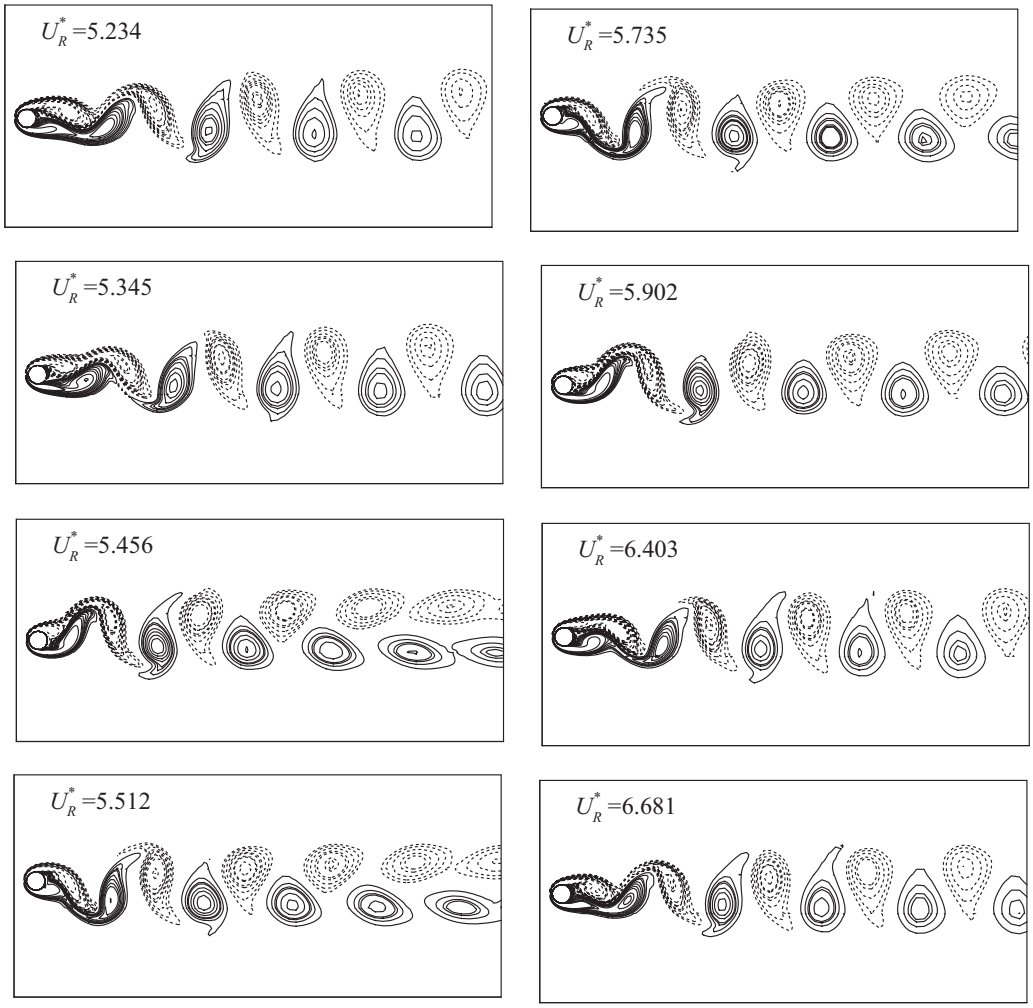

Fig. 5. Vortex shedding modes of the vibrating cylinder for various values of reduced velocity.

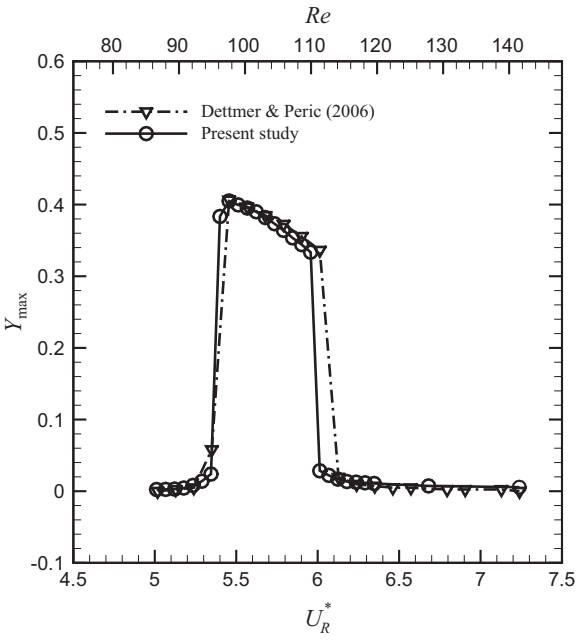

Fig. 6. Variation of the maximum transverse displacement of the vibrating cylinder with increasing reduced velocity.

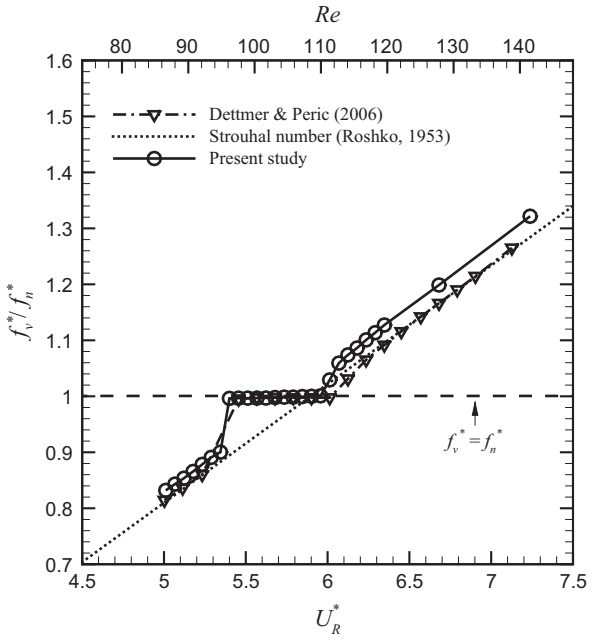

Fig. 7. Variation of the frequency ratio with increasing reduced velocity. The Strouhal number proposed by Roshko (1953) is defined by $St = 0.212(1-21.2/Re)$.

maximum value about 0.4D for $U_R^* \sim 5.45$ after $t^* \geq 2000$. Meanwhile, it indicates that the movement of the cylinder starts to synchronize with periodic force on the solid body. Williamson and Roshko (1988) defined several vortex shedding modes in detail. The definition of 2S mode is that two single vortices are formed in each cycle and released from the cylinder. Another vortex shedding mode 2P is given by that two vortex pairs are shed per cycle alternatively. According to the definition of vortex shedding mode, the 2S mode is observed in the present study as seen in Fig. 5. The alternatively shedding of vortices gives a dimensionless frequency, namely Strouhal number St. Variation in the system response with U_R^* is investigated and the results are summarized in Fig. 6. The present results show that our data are in good agreement with Dettmer and Peric (2006). It is found that before and beyond the lock-in region the vibration amplitude of the cylinder is very small. It is also noticeable that the maximum amplitude is found near the lower limit of the lock-in/synchronization region. Another evidence of the synchronization region can be seen in Fig. 7 where the vortex shedding frequency is obtained by an FFT analysis of C_L and normalized by the reduced natural frequency of structure. St for a stationary cylinder proposed by Roshko (1953) following the formula $St = 0.212(1 - 21.2/Re)$ is superimposed for comparison. It has been observed by a number of researchers in the past that in the lock-in region. Traditionally, the ratio of vortex shedding frequency to the natural frequency of structure is close to 1. For a range of values of U_R^* from 5.4 to 6.0, approximately, lock-in/synchronization phenomenon takes place in the present results. In the present study, the vortex shedding frequency of the vibrating cylinder exactly matches the natural frequency of the structure in the lock-in region and a strong evidence in the jump of the cylinder response is found in the low end of the synchronization region. Another interesting finding is that beyond or before the range of U_R^* for lock-in region, the vortex shedding frequency moves back to St for a stationary cylinder. These investigations are in good agreement with Williamson and Govardhan (2004).

The general trend of the lock-in region is captured well by the proposed model. Moreover, from the amplitude and the frequency responses of cylinder, it is found that the present results are almost consistent with the numerical work using the ALE method by Dettmer and Peric (2006).

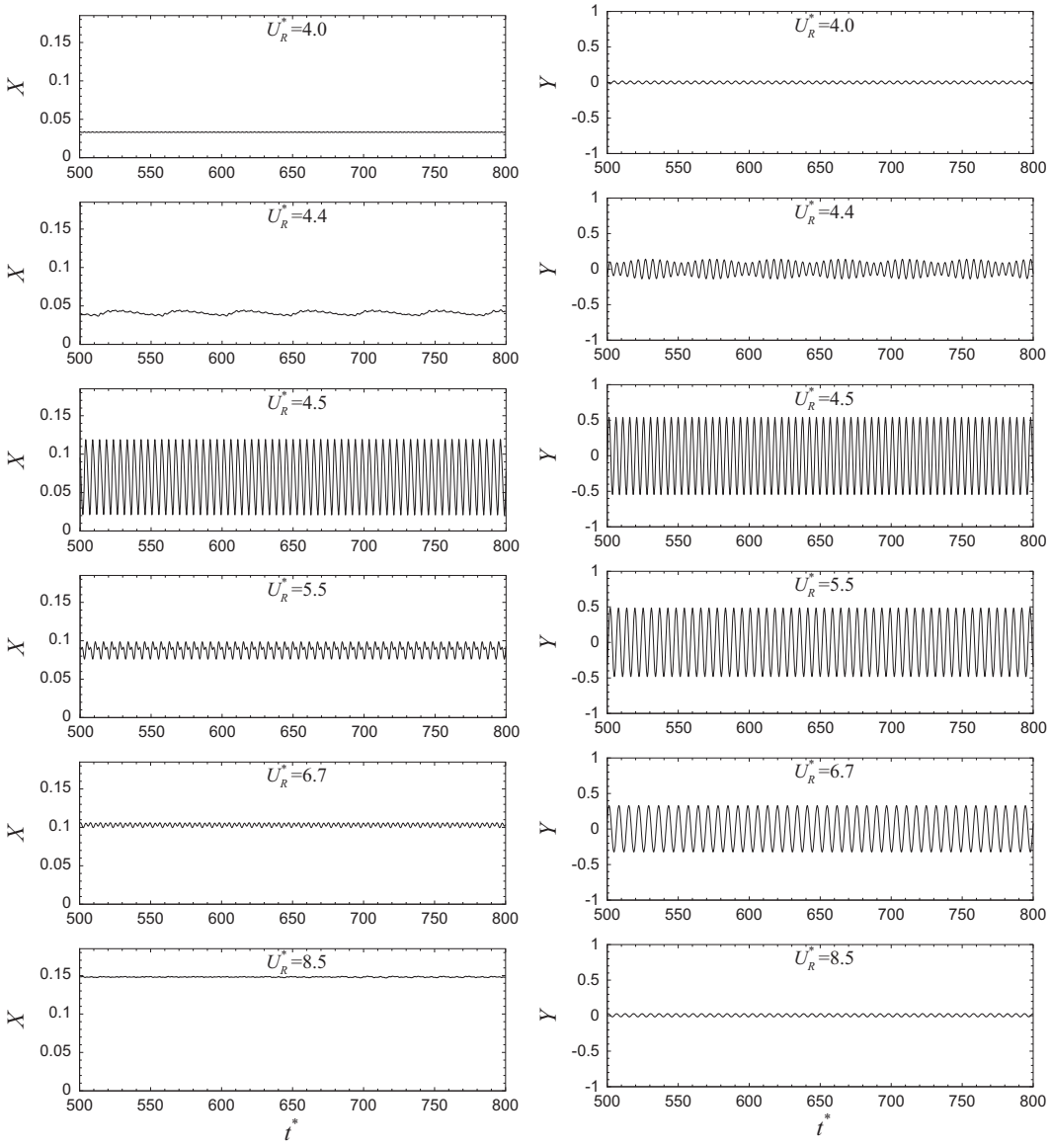

Fig. 8. Time history of the normalized in-line and transverse displacements of the vibrating cylinder for various values of reduced velocity.

3.2. In-line and transverse vibrations

Cylinder vibration in the transverse direction plays a significant role to the cylinder response than the in-line direction. It is well known in the VIV problems that a freely vibrating cylinder in the in-line direction has a little effect on the cylinder response. Typically, an in-line amplitude is significantly smaller than a transverse amplitude in VIV but their contributions to restricting fatigue life of the structure can be very important as explained by Bearman (2011). To further study the interaction between the in-line and the transverse responses of a freely vibrating cylinder, an elastically mounted cylinder in a uniform flow is considered. The cylinder is allowed to vibrate in two-degree-of-freedom at moderate *Re*. The system parameters are set according to the numerical works by Singh and Mittal (2005). The dimensionless mass m^* of the cylinder is 10. To reach a maximum amplitude vibration, the structural damping ratio ζ is set to zero. In experimental studies, the variation of U_R^* is achieved by varying the inlet velocity. In this sense, U_R^* and *Re* are independent parameters. In the present numerical model, *Re* is fixed at 100 and U_R^* varies from 4.0 to 8.5. The variation of U_R^* is achieved by altering the natural frequency of the structure.

3.2.1. Flow patterns and modes of vortex shedding

The time history of the normalized in-line and transverse displacements of the vibrating cylinder for various values of U_R^* is presented in Fig. 8. As shown in the figure, the amplitudes of transverse vibrations are significantly higher than those of the in-line vibrations. It can be found in those figures that the beating phenomenon exists in the time history of the normalized displacements of the vibrating cylinder at $U_R^* = 4.4$. As U_R^* goes beyond this point, the beating patterns change to the almost periodic standing wave with a maximum transverse amplitude of oscillations around $0.55D$ at $U_R^* = 4.5$. Also, the peak amplitude of vibrations in the in-line direction is observed at $U_R^* = 4.5$, approximately. Beyond a certain range of U_R^*, the amplitudes of oscillations in both directions become much smaller. Overview of literatures about a uniform flow past a stationary cylinder at $Re = 100$ as seen from Anagnostopoulos (1994), Shiels et al. (2001) and Singh and Mittal (2005), the 2S vortex shedding mode is found. The vibrating cylinder experiences a high amplitude oscillations and excites a different wake structure as seen in Fig. 9. Despite the vortex shedding is still in the 2S mode, the vorticity patterns are somehow different from the conventional 2S mode. The findings are in good agreement with numerical results reported by Singh and Mittal (2005) and Prasanth and Mittal (2008). They defined this pattern as the C(2S) mode of vortex shedding. A '2C' mode which comprises two co-rotating voices each half cycle was first defined by Flemming and Williamson (2005). The C(2S) mode is similar to that of the 2S mode except that vortices coalesce in the wake behind the body. In the present results, the range of U_R^* for the C(2S) mode is discovered from 4.5 to 5.0. Within this region, the

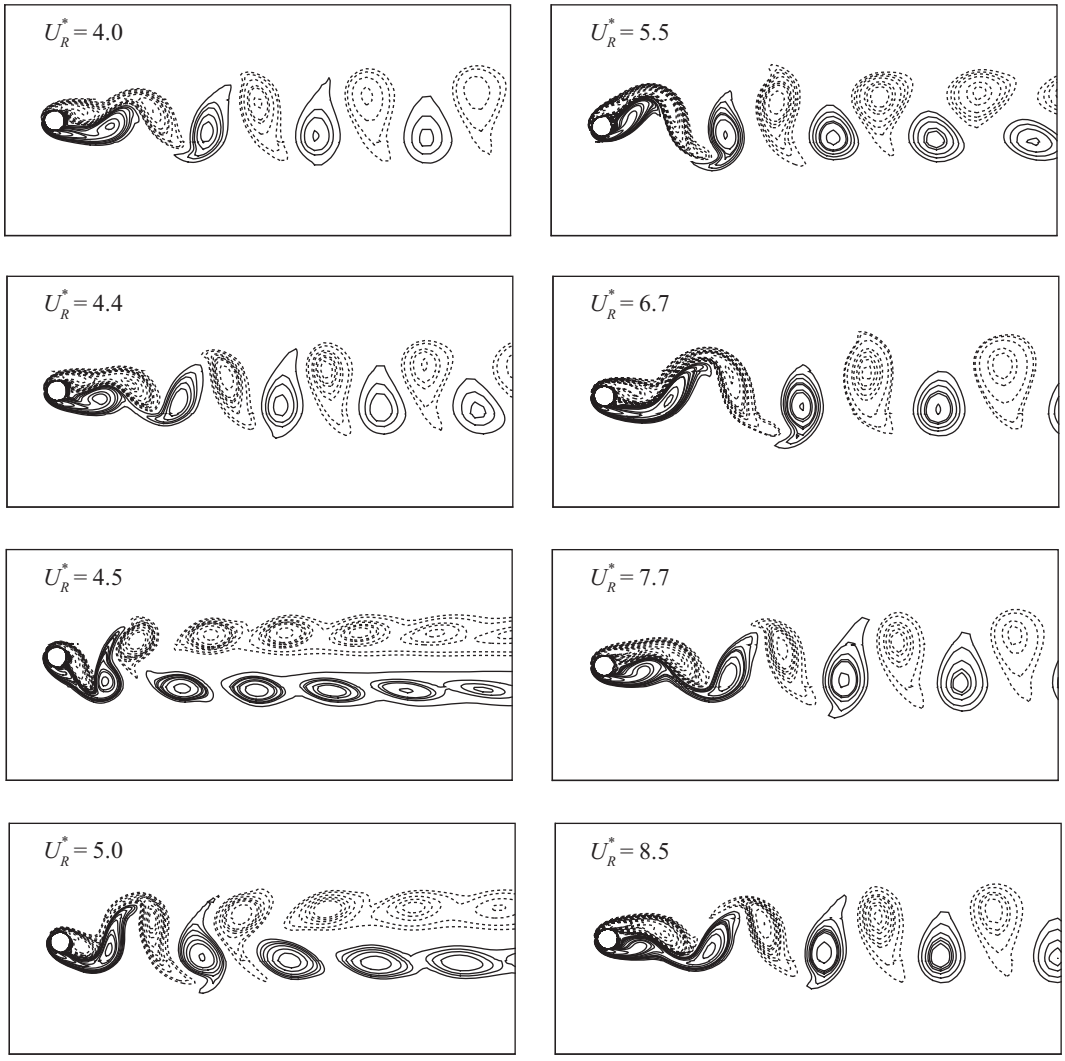

Fig. 9. Vortex shedding modes of the vibrating cylinder for various values of reduced velocity.

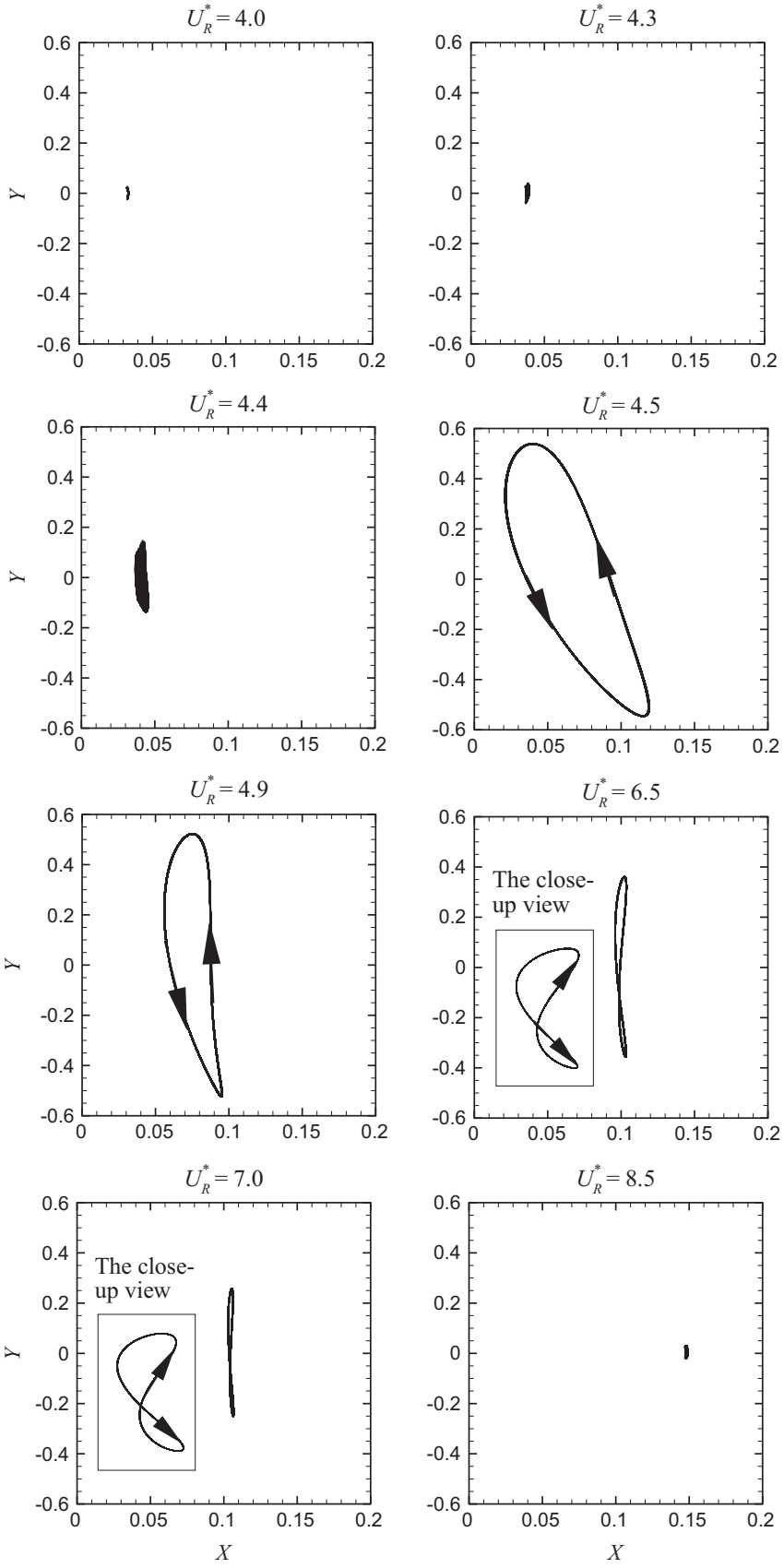

Fig. 10. Trajectory diagrams of the movement of the vibrating cylinder for various values of reduced velocity.

maximum amplitude decreases to 0.51D but still shows standing wave patterns. Out of this region, the wake structure comes back to the 2S vortex shedding mode. Furthermore, the low amplitude of vibrations of the cylinder exhibits the 2S mode of vortex shedding and occasionally, it is C(2S) when the oscillation amplitude is large. It is found that the vortex shedding mode depends on U_R^*.

According to the results obtained by the present numerical model, it is found that a periodic behavior exists for most of the cases. The trajectory diagrams indicate that the flow and the movement of the cylinder are periodic as shown in Fig. 10. Interestingly, the cylinder undergoes a slightly oval-shaped motion within the lock-in region roughly but a slightly eight-shaped motion in a range of U_R^* from 5.5 to 7.0. At the same time, the maximum transverse amplitude of vibrations descends from 0.48D to 0.26D. Also, the C(2S) vortex shedding mode vanishes at this range of U_R^* and it is replaced by the 2S vortex shedding mode. The attached video shows the vortex shedding patterns of the C(2S) and 2S modes and its corresponding trajectories.

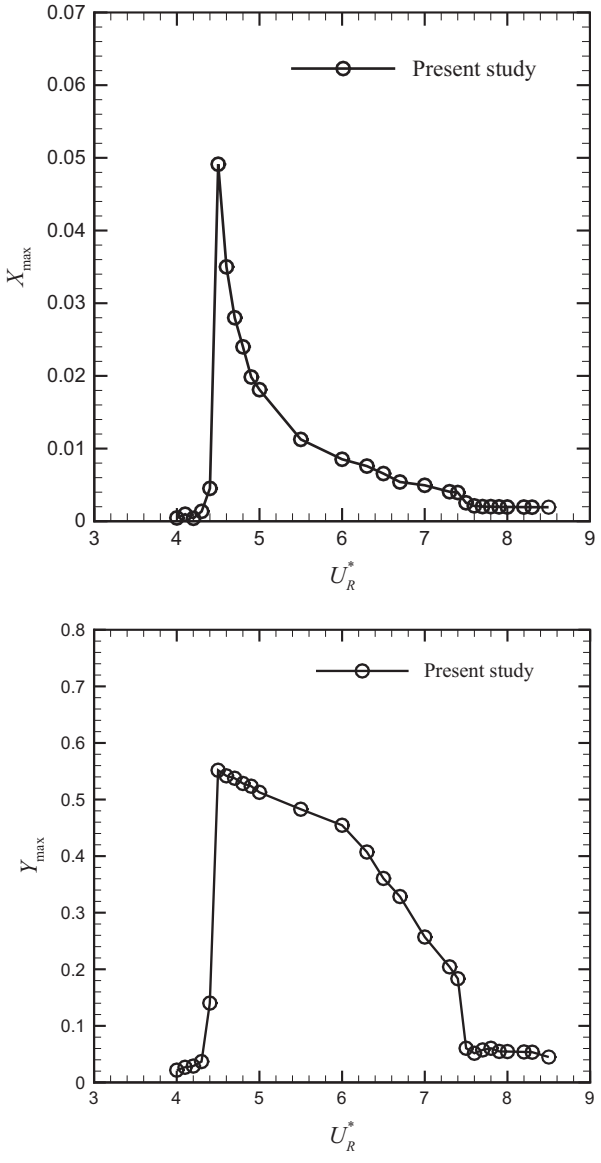

Fig. 11. Variation of maximum in-line and transverse displacements of the vibrating cylinder with increasing reduced velocity.

3.2.2. Influence of reduced velocity on the cylinder response

U_R^* is a non-dimensional parameter that consists of flow velocity u_∞, the natural frequency of the cylinder f_n and the cylinder's diameter D. The physical meaning of U_R^* is described in detail by Yang et al. (2009). It can be explained as the ratio of fluid force acting on the cylinder and the elastic restoring force of the cylinder. For VIV of the cylinder, U_R^* is a considerable parameter. Fig. 11 shows the variations of X_{max} and Y_{max} of a vibrating cylinder with U_R^*. It clearly indicates that when Re is fixed, U_R^* dominates the process of VIV of the cylinder. It can be seen that the amplitudes of the transverse vibrations are significantly higher than those of the in-line vibrations. In the present study, the peak amplitude of vibrations in the transverse direction is around 0.55D, which is within 5% discrepancy from that reported by Singh and Mittal (2005) and it is achieved for $U_R^* = 4.5$. The range of the lock-in/synchronization region takes place at $4.5 \le U_R^* \le 7.4$, approximately. It is also conspicuous that the maximum amplitude is found near the lower limit of the lock-in/synchronization region as same as the single-degree-of-freedom problem. The general response of the cylinder is very similar to the results reported by Singh and Mittal (2005). The cylinder response obtained from the present study is in good agreement with that reported by other researchers as summarized by Williamson and Govardhan (2004) except for the onset of the lock in region. Within the lock-in regime, the present study points out that the vortex shedding frequency is quite close to the natural frequency of the structure as shown in Fig. 12. Herein, the Strouhal number St is proposed by Roshko (1953) for a stationary cylinder. Interestingly, beyond or before the range of U_R^* for synchronization, the vortex shedding frequency moves back to that for a stationary cylinder($St \sim 0.166$). The variations of $\overline{C}_D$ and $C_{L,rms}$ for two-degree-of-freedom of an elastically mounted circular cylinder also show the jump behavior at the low end of the synchronization region as shown in Fig. 13. From the results of vibrations, compared to a stationary cylinder at $Re = 100$, $\overline{C}_D$ and $C_{L,rms}$ for out of the lock-in region are nearly 1.30 and 0.20. It is an evidence that our numerical results are very close to the data of stationary cylinder at $Re = 100$ as summarized in Table 2. Furthermore, it is found that beyond the lock-in region, the cylinder exhibits a small oscillation amplitude. Meanwhile, in the synchronization region, the cylinder experiences high aerodynamic forces that lead to large amplitudes of oscillation.

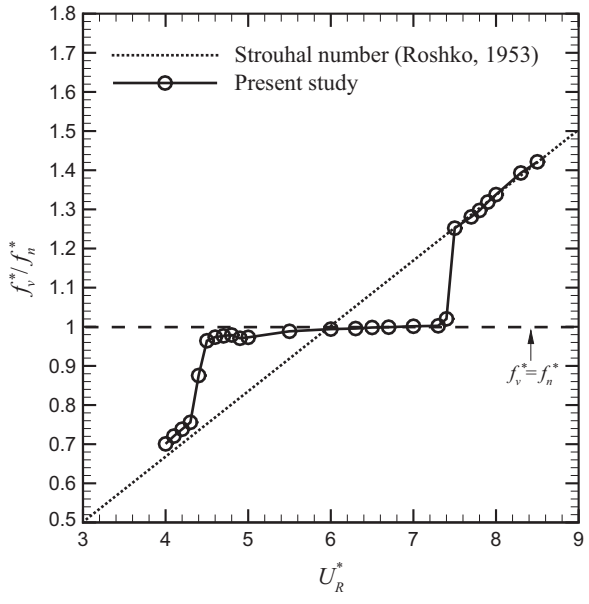

Fig. 12. Variation of the frequency ratio with increasing reduced velocity. The Strouhal number proposed by Roshko (1953) is defined by $St = 0.212(1 - 21.2/Re)$.

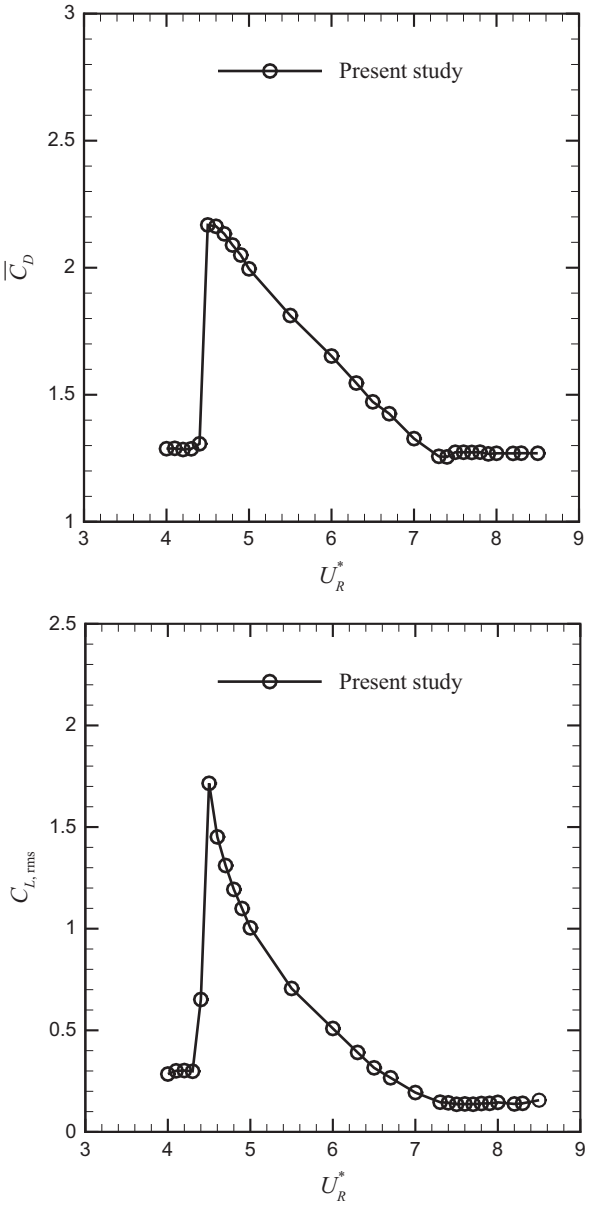

Fig. 13. Variation of the mean drag and r.m.s. values of lift coefficients of the vibrating cylinder with increasing reduced velocity.

Table 2
Comparison of results for a fixed cylinder at $Re=100$.

Author	$C_{L,\mathrm{rms}}$	$\overline{C}_D$	St
Anagnostopoulos (1994)	0.27	1.20	0.167
Shiels et al. (2001)	0.33	1.33	0.167
Singh and Mittal (2005)	0.25	1.35	0.163
Present study (vibrating cylinder)	0.20	1.30	0.166

4. Conclusions

Two-degree-of-freedom vortex-induced vibration (VIV) of a spring-mounted circular cylinder has been simulated successfully using the direct-forcing immersed boundary (DFIB) method. For two-degree-of-freedom VIV of the cylinder in a uniform stream, the peak oscillation amplitudes in both directions appear on the onset of lock-in/synchronization region. It is found that the amplitude response in the transverse direction is significantly higher than that of the in-line direction. Also, the hydrodynamic coefficients show the jump behavior at the low end of the lock-in region. Interestingly, the lock-in condition occurs in the slightly oval-shaped and eight-shaped orbits as shown in the trajectory diagrams of cylinder movement. From an analysis of the wake structure behind a freely vibrating cylinder in a laminar flow, it exhibits that the 2S mode is found at low oscillation amplitude of the cylinder. The C(2S) mode appears as the oscillation amplitude becomes large. Moreover, it is noted that beyond or before the range of U_R^* for the synchronization region, the vortex shedding frequency becomes the same value of a fixed cylinder.

Numerical simulations for an elastically mounted circular cylinder which is allowed to vibrate in both directions have showed that the present DFIB method has a good capability to handle complex VIV problems. In summary, the general trend of the lock-in region, cylinder movement, vortex shedding mode, amplitude and frequency responses are predicted reasonably.

Acknowledgments

The authors would like to express their gratitude for the financial support from National Science Council, Taiwan (No. NSC 102-2212-E-011-042).

Appendix A. Supplementary material

Supplementary data associated with this article can be found in the online version at http://dx.doi.org/10.1016/j.jweia.2014.08.015.

References

Anagnostopoulos, P., 1994. Numerical investigation of response and wake characteristics of a vortex excited cylinder in a uniform stream. J. Fluids Struct. 8, 367–390.
Bearman, P.W., 1984. Vortex shedding from oscillating bluff bodies. Annu. Rev. Fluid Mech. 16, 195–222.
Brika, D., Laneville, A., 1993. Vortex-induced vibrations of a long flexible circular cylinder. J. Fluid Mech. 250, 481–508.
Bernitsas, M.M., Raghavan, K., Ben-Simon, Y., Garcia, E.M.H., 2008. VIVACE (Vortex Induced Vibration Aquatic Clean Energy): a new concept in generation of clean and renewable energy from fluid flow. J. Offshore Mech. Arct. Eng., ASME Trans. 130, 041101–041115.
Blevins, R.D., Coughran, C.S., 2009. Experimental investigation of vortex-induced vibration in one and two dimensions with variable mass, damping, and Reynolds Number. J. Fluids Eng. 131, 101202–101203.
Bearman, P.W., 2011. Circular cylinder wakes and vortex-induced vibrations. J. Fluids Struct. 27, 648–658.
Chern, M.J., Hsu, W.C., Horng, T.L., 2012. Numerical prediction of hydrodynamic loading on circular cylinder array in oscillatory flow using direct-forcing immersed boundary method. J. Appl. Math., 2012, 16 p (Article ID 505916). http://dx.doi.org/10.1155/2012/505916.
Chern, M.J., Hsu, W.C., Horng, T.L., 2013. Numerical study for interaction of oscillatory flow with cylinder array using immersed boundary method. J. Fluids Struct. 43, 325–346.
Dettmer, W.G., Perić, D., 2006. A computational framework for fluid rigid body interaction: finite element formulation and applications. Comput. Methods Appl. Mech. Eng. 195, 1633–1666.
Feng, C.C., 1968. The Measurement of Vortex Induced Effects in Flow Past Stationary and Oscillating Circular and D-Section Cylinders (Master thesis). University of British Columbia, Vancouver, Canada.
Flemming, F., Williamson, H.K., 2005. Vortex-induced vibrations of a pivoted cylinder. J. Fluid Mech. 522, 215–252.
Govardhan, R., Williamson, C.H.K., 2000. Modes of vortex formation and frequency response for a freely-vibrating cylinder. J. Fluid Mech. 420, 85–130.
Guilmineau, E., Queutey, P., 2004. Numerical simulation of vortex-induced vibration of a circular cylinder with low mass-damping in turbulent flow. J. Fluids Struct. 19, 449–466.
Hirt, C., Nickols, B., Romero, N., 1975. A numerical solution algorithm for transient fluid, LA-5852. Los Alamos Scientific Laboratory, Los Alamos, New Mexico, USA.
Kuyper, R., Meer, T.V.D., Hoogendoorn, C., Henkes, R., 1993. Numerical study of laminar and turbulent natural convection in an inclined square cavity. Int. J. Heat Mass Transf. 36 (11), 2899–2911.
Khalak, A., Williamson, C.H.K., 1996. Dynamics of a hydroelastic cylinder with very low mass and damping. J. Fluids Struct. 10, 455–472.

Khalak, A., Williamson, C.H.K., 1997a. Fluid forces and dynamics of a hydroelastic structure with very low mass and damping. J. Fluids Struct. 11, 973–982.
Khalak, A., Williamson, C.H.K., 1997b. Investigation of relative effects of mass and damping in vortex-induced vibration of a circular cylinder. J. Wind Eng. Ind. Aerodyn. 71, 341–350.
Khalak, A., Williamson, C.H.K., 1999. Motions, forces and mode transitions in vortex-induced vibrations at low mass-damping. J. Fluids Struct. 13, 813–851.
Leonard, B.P., 1979. A stable and accurate convective modelling procedure based on quadratic upstream interpolation. Comput. Methods Appl. Mech. Eng. 19, 59–98.
Leontini, J.S., Thompson, M.C., Hourigan, K., 2006. The beginning of branching behaviour of vortex-induced vibration during two-dimensional flow. J. Fluids Struct. 22, 857–864.
Luo, H., Dai, H., Ferreira de Sousa, P.J.S.A., Yin, B., 2012. On the numerical oscillation of the direct-forcing immersed-boundary method for moving boundaries. Comput. Fluids 56, 61–76.
Lee, J., You, D., 2013. An implicit ghost-cell immersed boundary method for simulations of moving body problems with control of spurious force oscillations. J. Comput. Phys. 233, 295–314.
Mohd. Yusof, J., 1996. Interaction of Massive Particles with Turbulence (Ph.D. thesis). Cornell University, USA.
Noor, D.Z., Chern, M.J., Horng, T.L., 2009. An immersed boundary method to solve fluid–solid interaction problems. Comput. Mech. 44, 447–453.
Peskin, C.S., 1972. Flow patterns around heart valves: a numerical method. J. Comput. Phys. 10, 252–271.
Parkinson, G., 1989. Phenomena and modelling of flow-induced vibrations of bluff bodies. Progr. Aerosp. Sci. 26, 169–224.
Prasanth, T.K., Mittal, S., 2008. Vortex-induced vibrations of a circular cylinder at low Reynolds numbers. J. Fluid Mech. 594, 463–491.
Roshko, A., 1953. On the development of turbulent wakes from vortex streets, NACA TN 2913.
Sarpkaya, T., 1979. Vortex-induced oscillations. J. Appl. Mech. 46, 241–258.
Shiels, D., Leonard, A., Roshko, A., 2001. Flow-induced vibration of a circular cylinder at limiting structural parameters. J. Fluids Struct. 15, 3–21.
Singh, S.P., Mittal, S., 2005. Vortex-induced oscillations at low Reynolds numbers: hysteresis and vortex-shedding modes. J. Fluids Struct. 20, 1085–1104.
Sotiropoulos, F., Yang, X., 2014. Immersed boundary methods for simulating fluid–structure interaction. Progr. Aerosp. Sci. 65, 1–21.
Williamson, C.H.K., Roshko, A., 1988. Vortex formation in the wake of an oscillating cylinder. J. Fluids Struct. 2, 355–381.
Williamson, C.H.K., Govardhan, R., 2004. Vortex-induced vibrations. Annu. Rev. Fluid Mech. 36, 413–455.
Wang, Z., Fan, J., Luo, K., 2008. Combined multi-direct forcing and immersed boundary method for simulating flows with moving particles. Int. J. Multiph. Flow 34, 283–302.
Yang, B., Gao, F., Jen, D.T., Wu, Y., 2009. Experimental study of vortex-induced vibrations of a cylinder near a rigid plane boundary in steady flow. Acta Mech. Sin. 25 (1), 51–63.